10A.2 Radar Differential Phase Signatures of Ice Orientation for the Prediction of Lightning Initiation and Cessation

Lawrence D. Carey[1*], Walter A. Petersen[2], and Wiebke K. Deierling[1]

[1] Earth System Science Center, NSSTC, University of Alabama in Huntsville, Huntsville, AL
[2] NASA Marshall Space Flight Center, Earth Sciences Office, VP-61, NSSTC, Huntsville AL

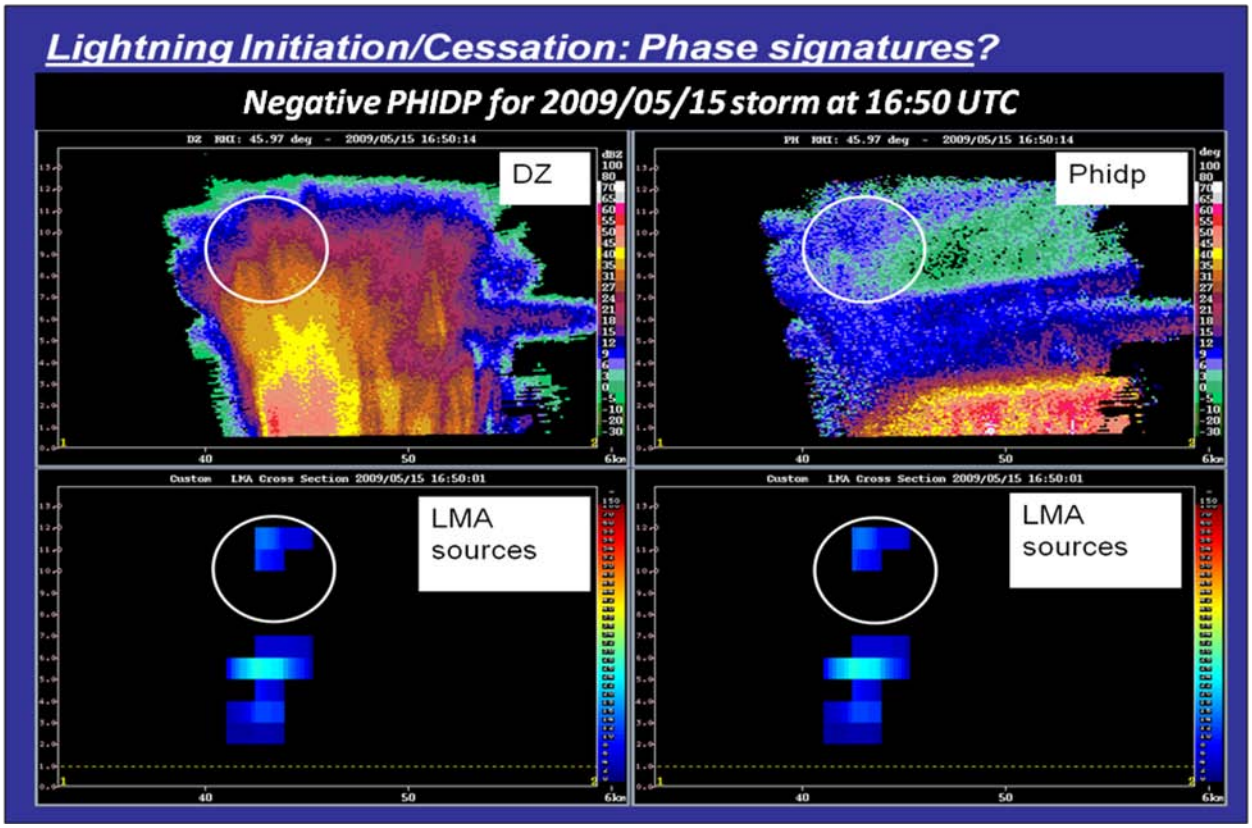

Figure 1. RHI (height km versus range km) of UAHuntsville-NASA ARMOR (Advanced Radar for Meteorological and Operational Research) dual-polarimetric radar signatures (upper panels) of ice crystal alignment likely caused by a strong electric field in a thunderstorm and associated NASA LMA (Lightning Mapping Array) VHF lightning sources (lower panels) over Northern Alabama. Upper-left: radar reflectivity (DZ, dBZ, shaded); Upper-right: differential propagation phase (Phidp, degrees, shaded), Lower-left (and lower-right repeated): VHF lightning sources. The negative differential phase (blue to green transition inside circle) is likely associated with vertically oriented ice crystals in a strong electric field. The strong electric field in the thunderstorm also likely caused the collocated lightning seen by the LMA inside the circled region.

1. INTRODUCTION

The 45th Weather Squadron (45 WS) provides weather support to America's space program at Cape Canaveral Air Force Station (CCAFS), NASA's Kennedy Space Center (KSC), and Patrick AFB (PAFB) in east central Florida. The weather support requirements of the space program are very stringent (Harms et al. 1999). Since central Florida experiences the largest annual cloud-to-ground lightning flash density in the U.S. (Huffines and Orville 1999), the short-term prediction of lightning initiation and cessation is a critical mission function for 45 WS in order to insure safe, successful operations at CCAFS/KSC. The 45 WS recently acquired a powerful new meteorological sensor to be employed toward this objective – the Radtec TDR 43-250 Doppler and dual-polarimetric radar (Roeder et al. 2009, this conference). NASA MSFC and the University of Alabama in Huntsville (UAHuntsville) are working

Corresponding author address: Dr. Lawrence D. Carey, ESSC/NSSTC, 320 Sparkman Dr., Huntsville, AL 35805; email: larry.carey@nsstc.uah.edu

collaboratively with 45 WS to explore the use of dual-polarimetric radar signatures to complement and supplement traditional radar-reflectivity based techniques (Roeder and Pinder 1998) for the operational prediction of lightning initiation and cessation.

To accomplish these applied research goals with 45 WS, UAHuntsville and NASA MSFC will leverage their experience in dual-polarimetric radar studies of thunderstorms and lightning production (e.g., Carey and Rutledge 1996; Deierling et al. 2005) and their observational capabilities in Northern Alabama such as the UAHuntsville-NASA ARMOR (Advanced Radar for Meteorological and Operational Research; Petersen et al. 2005) and NASA MSFC Lightning Mapping Array (LMA).

2. BACKGROUND AND MOTIVATION

Small ice crystals up to 1-2 mm can be vertically aligned by strong vertical electric fields of about 100-200 kV m^{-1} (Weinheimer and Few 1987). Smaller crystals are easier to align while the larger ice crystals will only by aligned in the strongest electric fields found in thunderstorms. Even larger ice hydrometeors such as aggregates and graupel likely do not align in strong electric fields. Ice crystal orientation signatures have been noted in polarimetric radar observations for a number of years (Hendry and McCormick 1976, McCormick and Hendry 1979; Hendry and Antar 1982; Krehbiel et al. 1991, 1992, 1993, 1996; Metcalf 1992, 1995). More recently, ice alignment signatures in differential propagation phase have been noted (Caylor and Chandrasekar 1996; Galloway et al. 1997; Scott et al. 2001; Marshall et al. 2009). In a research setting, dual-polarimetric radar signatures of ice alignment have been used to indicate the potential for lightning, predict the occurrence of numerous lightning discharges, anticipate the initial electrification of storms, and determine when a storm is finished producing lightning (Krehbiel et al. 1993, 1996).

Radar differential propagation phase parameters (specific differential phase, K_{dp}, and its integral ϕ_{dp} or PHIDP) are currently measured by research (e.g., UAHuntsville and NASA MSFC ARMOR C-band) and operational (e.g., CCAFS-KSC Radtec TDR 43-250 C-band) radars. An example of an ice orientation signature in ARMOR PHIDP measurements associated with LMA lightning in a typical thunderstorm over Northern Alabama is shown in Fig. 1.

Radar differential phase (K_{dp}, PHIDP) signatures of ice orientation depend on radar characteristics (e.g., frequency, elevation angle, phase stability), the magnitude of the vertical electric field, which controls ice orientation angle, and ice hydrometeor properties in the radar resolution volume (ice particle type, shape, size, concentration, density, and orientation). The purpose of this study is to investigate these three key issues in order to develop better operational radar-based tools for the prediction of lightning potential. The overall approach is to employ polarimetric radar observations and modeling of differential phase (K_{dp}, PHIDP) and other polarimetric variables routinely available from UAHuntsville-NASA ARMOR and 45 WS Radtec radars.

Although there is substantial past work on the modeling of dual-polarimetric radar properties of ice particles (e.g., Matrosov 1991, Vivekanandan et al. 1993 and 1994, Matrosov et al. 1996, Ryzhkov et al. 1998), little attention has been given to the problem of vertically oriented ice in the context of lightning potential. One exception is Caylor and Chandrasekar (1996) who presented detailed dual-polarimetric observations just prior to, during, and after individual lightning flashes. Caylor and Chandrasekar (1996) also modeled K_{dp} for horizontally oriented idealized plates and columns. In their modeling efforts, they did not treat vertically oriented ice crystals nor was there any treatment of ice mixtures.

The focus of this paper is on modeling the effects of ice particle size distribution, ice canting angle in response to an electric field, ice crystal type, ice aggregate properties, graupel properties and mixtures of different ice types (e.g., crystals and aggregates, crystals and graupel) on dual-polarimetric radar parameters, especially K_{dp}. Treatment of ice mixtures is required to understand the behavior of the differential reflectivity (Z_{dr}), which is a measure of the reflectivity-weighted shape of hydrometeors, and likely K_{dp} as well.

In fact, we explore whether the presence of larger, unaligned particles such as aggregates and graupel in the radar resolution volume can influence the K_{dp}-signature associated with vertically oriented ice crystals. According to Marshall et al. (2009), "*electrical alignment of ice crystals is indicated by the change in PHIDP along each radar beam…observing an alignment signature requires that larger, unaligned particles are absent (since they would mask the alignment signature)*." If and when true, the efficacy of the alignment signature would be reduced because microphysical conditions potentially unrelated to the electric field strength and lightning potential

would modify PHIDP and K_{dp} (i.e., and hence potentially mask the alignment signature). We test the hypothesis of Marshall et al. (2009) and determine under what conditions the alignment signature could be masked.

3. GENERAL METHODOLOGY

Complex shapes of ice particles are modeled as oblate (O) or prolate (P) spheroids (Matrosov 1991, Vivekanandan et al. 1993 and 1994, Matrosov et al. 1996, Caylor and Chandrasekar 1996, Ryzhkov et al. 1998). Ice particle types are selected for their relevance to the upper-portions of thunderstorm cells and associated anvils (Heymsfield 1986, Garrett et al. 2005) such as plate (O), dendrites (O), columns (P), aggregates (O/P), and graupel (O/P). Following the radar studies of ice particles listed above, we model reasonably realistic particle size distributions, densities, shapes and orientations according to the microphysical literature (Auer and Veal 1970, Heymsfield 1972, Pruppacher and Klett 1997).

Scattering by and propagation in ice particles are modeled using the T-matrix (Waterman 1969) approach at radar wavelengths from S- to Ka-band, although we focus on C-band results in this paper because of the ARMOR and CCAFS/KSC radars. Radar parameters such as the horizontal radar reflectivity (Z_h), differential reflectivity (Z_{dr}), specific differential phase (K_{dp}), co-polar correlation coefficient (ρ_{hv}), linear depolarization ratio (LDR), specific attenuation (A_h), and specific differential attenuation (A_{hv}) of ice particle mixtures, including the effects of particle orientation and radar elevation angle, are calculated using the Mueller matrix-based approach of Vivekanandan et al. (1991). In this paper, we focus on Z_h, Z_{dr} and especially K_{dp}. Particle orientation is modeling using a Gaussian distribution of canting angles with a prescribed mean and standard deviation (σ) for each particle type. Although radar elevation angle is modeled, we present results at 0° radar elevation angle in this paper for simplicity sake.

4. RESULTS

4.1 Dependence of K_{dp} on Ice Particle Size Distribution

We model the particle size distribution (PSD) of all ice hydrometeor types (including ice crystals, aggregates and graupel) according to the exponential distribution: N(D)=N0*exp(-3.67*D/D0) where D is equivalent diameter, N0 is the intercept parameter, D0 is the median volume diameter, and 3.67/D0 is the slope parameter (Pruppacher and Klett 1997). To explore the sensitivity of K_{dp} to variations in the PSD parameters, hexagonal plates are modeled first. The PSD parameters (N0 and D0) are varied as follows: $2\times10^5 m^{-3}\ cm^{-1} \le N0 \le 2\times10^6 m^{-3}\ cm^{-1}$ and $0.03 \le D0 \le 0.07$ cm (D_{max} = 0.11 cm). The plate shape is approximated as an oblate spheroid. The shape (minor-to-major axis ratio) is calculated as a function of D according to Auer and Veal (1970). Ice density of plates as a function of D is specified according to Heymsfield (1972). For this PSD sensitivity test, the hexagonal plates are vertically oriented (canting angle for an oblate = 90°), as in a strong electric field. All radar simulations shown here and throughout the rest of the paper are calculated at C-band (5.625 GHz, 5.33 cm).

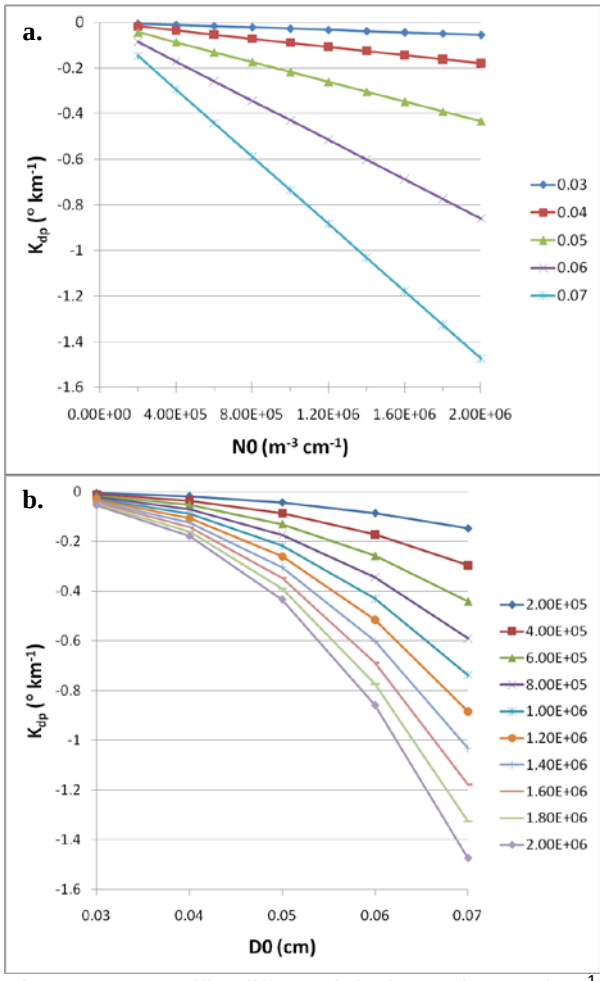

Figure 2. Specific differential phase (K_{dp}, ° km^{-1}) versus the parameters of an exponential size distribution. a. K_{dp} vs. N0 (m-3 cm-1) for various fixed values of D0 (see key to right) and b. K_{dp} vs. D0 for various fixed values of N0 (see key to right).

As seen in Fig. 2a, K_{dp} of vertically oriented plates is linearly proportional to particle concentration or the intercept parameter (N0) of an exponential size distribution, similar to the results of Vivekanandan et al. (1994) in horizontally oriented ice crystals. K_{dp} is non-linearly related to particle size or D0 (Fig. 2b). In summary, K_{dp} increases (decreases) linearly for increasing (decreasing) particle concentrations and non-linearly for increasing (decreasing) sizes. In other words, the K_{dp} ice crystal alignment signature could potentially change independent of the particle orientation angle and any influence of the electric field as a result of microphysical processes that modify N0 and D0.

Although not modeled here, this PSD effect would be further complicated by the fact that the orientation angle of each ice crystal type is a function of both the electric field strength and the particle size (Weinheimer and Few 1987). We assumed here that the plates are vertically oriented (i.e., D is small enough and the electric field is strong enough to orient the ice crystal in the vertical).

4.2 K_{dp} and Z_{dr} Dependence on Mean Ice Particle Canting Angle

To test the sensitivity of K_{dp} and Z_{dr} to changes in the mean ice particle canting angle, plates are modeled as oblate spheroids at C-band as before but for a single case with relatively large (D0 = 0.07 cm) and highly concentrated (N0 = $2x10^6$ m^{-3} cm^{-1}) particles. The mean canting angle for the oblate plate is then varied from 0° (horizontally oriented) to 90° (vertically oriented) (with a standard deviation of canting angle ≈ 0°) (Fig. 3).

As expected, K_{dp} and Z_{dr} swing from large positive values to large negative values as the canting angle changes from 0° to 90°. The lack of mirror symmetry in the polarimetric variables about the 45° mean canting angle (cf. Z_{dr} and K_{dp} at 0° vs. 90°) is related to the random orientation of the oblate spheroids in the 2nd angular direction (i.e., the canting angle distribution is assumed Gaussian in θ and random in ϕ as depicted in Fig. 1 of Vivekanandan et al. 1991). For this assumption, horizontally oriented oblates tend to have a larger absolute magnitude of Z_{dr} and K_{dp} than vertically oriented oblates. Although not shown, the effect is the reverse for prolate ice particles. The assumption of random orientation in the ϕ-direction is a reasonable modeling approach at low elevation angles since ice would not have a preferred orientation in this direction unless there is a strong horizontal electric field.

Clearly, K_{dp} and Z_{dr} are a strong function of the mean canting angle (Fig. 3), which will depend on the electric field strength, particle size, particle shape, and particle density (Weinheimer and Few 1987). Each ice particle type will have a critical electric field threshold that must be exceeded in order to orient them into the vertical. These electric field thresholds are not well known but are order 10-100 kV m^{-1} for most small ice crystals (< 1-2 mm) (Weinheimer and Few 1987).

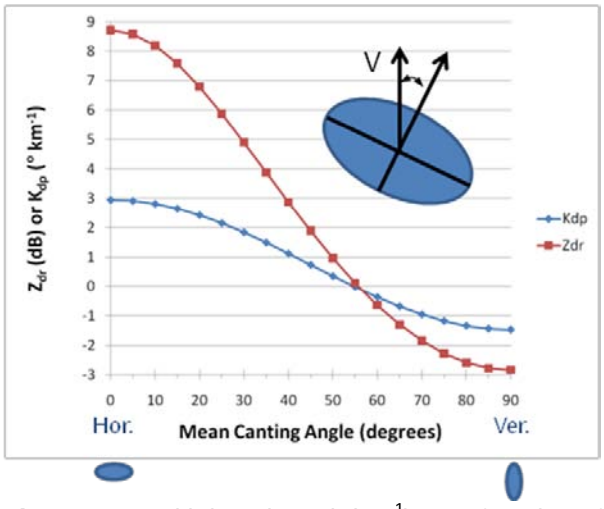

Figure 3. Z_{dr} (dB) and K_{dp} (° km^{-1}) as a function of the mean canting angle (depicted graphically in the inset) for oblate plate-type crystals with an exponential PSD for which N0 = $2x10^6$ m^{-3} cm^{-1} and D0 = 0.07 cm.

4.3 K_{dp} and Z_{dr} Dependence on Ice Crystal Type

The sensitivity of Z_{dr} vs. Z_h (Fig. 4a) and K_{dp} vs. Z_h (Fig. 4b) to ice crystal type is explored by using similar PSD (with range of N0 and D0 given in Section 4.1), shape (Auer and Veal 1970), density (Heymsfield 1972), radar wavelength (C-band), and vertical orientation assumptions as described earlier for plates (O), dendrites (O) and columns (P).

As shown in Fig. 4a, Z_{dr} depends on particle type but varies between about -3 and -5 dB for vertically oriented ice crystals. For the range of ice crystal sizes tested, Z_{dr} is a strong function of Z_h for dendrites only while Z_{dr} for plates and columns show little variation with Z_h. The behavior of Z_{dr} vs. Z_h is related to the size (D0) versus shape relation of each hydrometeor within the size range tested. For single particle types, Z_{dr} is independent of N0.

K_{dp} decreases from 0 to -1.2 to -1.6° km^{-1}, depending on crystal type as Z_h increases from about -12 dB to 22 dB (Fig. 4b). As expected from Section 4.1, the relationship between K_{dp} and Z_h is primarily a strong a function of N0 (concentration) and D0 (size). K_{dp} is less sensitive to crystal type than Z_{dr}. Behavior of K_{dp} vs. Z_h depends modestly on ice crystal type. The difference is mostly density difference driven. For a given Z_h, the K_{dp} of plates and columns are about the same while the K_{dp} for dendrites is 15-30% less).

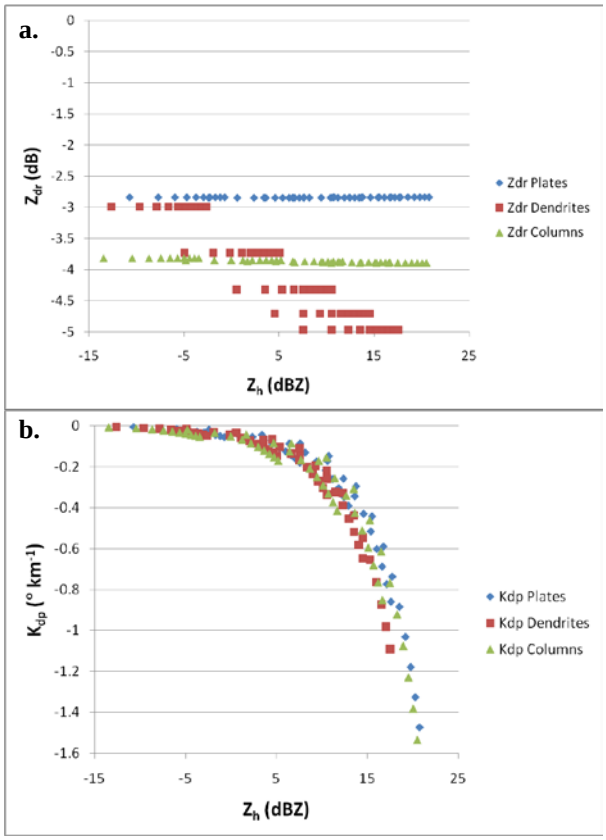

Figure 4. The sensitivity of dual-polarimetric parameters vs. Z_h as a function of ice crystal type (plates, dendrites and columns as shown in key to the right). a. Z_{dr} (dB) vs. Z_h (dBZ) and b. K_{dp} (° km^{-1}) vs. Z_h (dBZ).

4.4 K_{dp} and Z_{dr} Dependence on Ice Aggregate Properties

Ice aggregates are modeled at C-band in a similar fashion as ice crystals. Aggregates are modeled as oblate spheroids with an exponential distribution of the PSD but with 1×10^4 m^{-3} cm^{-1} ≤ N0 ≤ 1×10^5 m^{-3} cm^{-1} and 0.3 ≤ D0 ≤ 0.7 cm (D_{max} = 1.5 cm). Ice density of aggregates is calculated as a function of size according to Brown and Francis (1995). The shape of aggregates is highly variable. To represent this range of variability in aggregate shape, the axis ratio of an oblate spheroid is set to either 0.3 or 0.8 as in Matrosov et al. (1996). Aggregate orientation is modeled as either horizontal (H) or vertical (V). Although it is likely that aggregates typically fall with their major dimension in the horizontal (H) and are too big to be oriented vertically (V) in a strong electric field, we explore both options since it is possible that the low density of some aggregates allow them to be oriented vertically in a strong field despite their larger size.

When the aggregates are falling with their major dimension in the horizontal (H: mean canting angle = 0°), they likely wobble about the mean. To model wobbling or canting aggregates, we set the standard deviation of the canting angle (σ) of H-mode particles to either 5° (slight wobbling) or 30° (moderate wobbling). V-mode (mean canting angle = 90°) aggregates are assumed to be under the influence of a strong vertical electric field and so σ is set to about 0°.

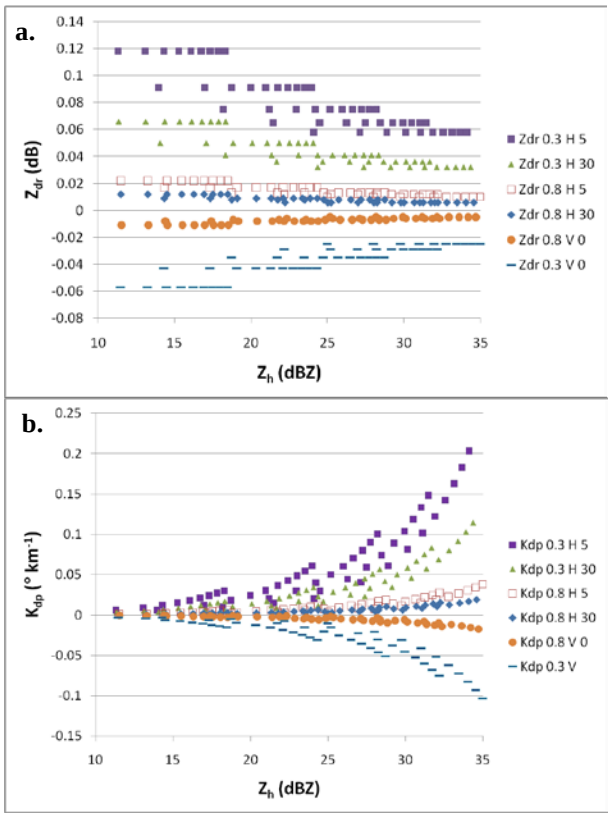

Figure 5. Dual-polarimetric parameter vs. Zh for aggregates of different types as shown in the key to the right (axis ratio, orientation, standard deviation of canting angle). See text for more details. a. Z_{dr} (dB) vs. Z_h (dBZ) and b. K_{dp} (° km^{-1}) vs. Z_h (dBZ).

The results for aggregates are shown in Fig 5a (Z_{dr} vs Z_h) and Fig. 5b (K_{dp} vs. Z_h). For a given radar reflectivity, more oblate (a/b=0.3) and less wobbling (σ =5°) particles have larger K_{dp} and Z_{dr} signatures, as expected. Z_{dr} tends to decrease slightly with increasing Z_h because of density dependence with size (Fig. 5a). K_{dp} tends to increase slightly for increasing Z_h due to the N0 and D0 dependence shown earlier (Fig. 5b). Overall, the K_{dp} and Z_{dr} responses to H- or V-oriented low density aggregates are significantly less than most pristine ice crystals because of the low density of aggregates (cf. Figs 4 and 5). If aggregates orient vertically in a strong electric field, the dual-polarimetric signatures would likely be comparably be weak. Horizontally oriented aggregates should not strongly mask K_{dp} orientation signatures of ice crystals in a mixture of crystals and aggregates. This hypothesis is explored in detail in the next section.

4.5 K_{dp} and Z_{dr} in Mixture of V-oriented Plates and H-oriented Aggregates

The dual-polarimetric radar properties of a mixture of vertically oriented (V-oriented) plates (Secs. 4.1 and 4.3) and horizontally oriented (H-oriented) aggregates (Sec. 4.4) assuming a/b = 0.3 and σ = 30° were calculated at C-band. Z_{dr} vs. Z_h of the aggregate-plate ice mixture along with aggregates only and plates only are shown in Fig. 6a. A similar plot of K_{dp} vs. Z_h of the aggregate-plate ice mixture along with aggregates only and plates only are shown in Fig. 6b. For a given value of Z_h, note that the K_{dp} and Z_{dr} of the ice mixture is bounded on both sides by the aggregate only and plate only values.

As Z_h increases and aggregates increasingly dominate the Z_h of the ice mixture, the Z_{dr} is driven toward the aggregate only value (near 0 dB) (Fig. 6a). The reflectivity-weighted behavior of Z_{dr} in an ice mixture is clearly shown in Fig. 7 in which Z_{dr} of the ice mixture is plotted as a function of the radar reflectivity fraction of aggregates (f_{Za}). As f_{Za} increases from 0 to 1, Z_{dr} of the ice mixture increases from the plate only value of near -3 dB to the aggregate only value of near 0 dB. Taken together, Figs. 6a and 7 clearly demonstrate that Z_{dr} is a poor indicator of electrical alignment because larger, H-oriented aggregates dominate the smaller, V-oriented plates.

Note that K_{dp} is nearly independent of Z_h in an ice mixture of V-oriented plates and H-oriented aggregates (Fig. 6b) because plates dominate K_{dp} behavior while aggregates dominate Z_h behavior. K_{dp} of an aggregate and plate ice mixture does not vary substantially from K_{dp} of plates only (Fig. 8). In other words, K_{dp} of low density H-oriented aggregates does not mask K_{dp} of V-oriented plates. In summary, K_{dp} is a good indicator of electrical alignment because smaller, V-oriented ice crystals dominate over larger, H-oriented aggregates.

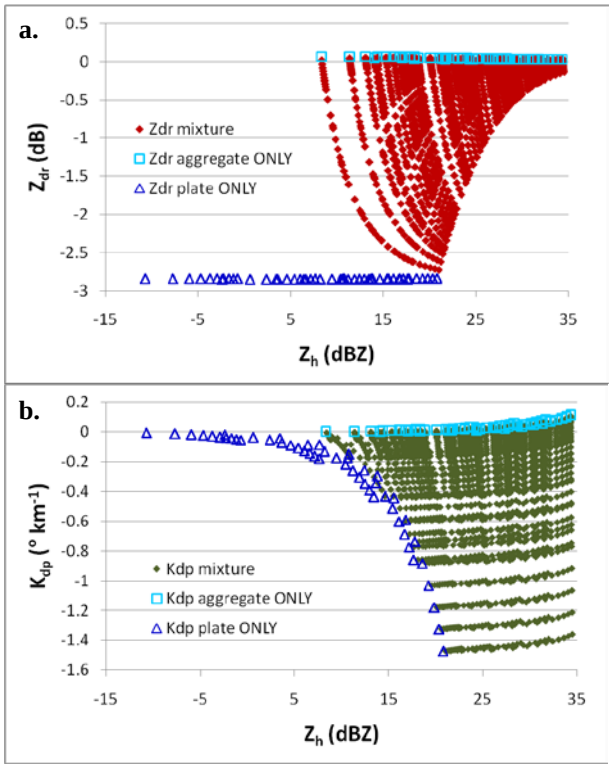

Figure 6. Dual-polarimetric parameter versus Zh in an ice mixture of H-oriented aggregates and V-oriented plates. a. Z_{dr} (dB) vs. Z_h (dBZ) and b. K_{dp} (° km^{-1}) vs. Z_h (dBZ). The dual-polarimetric parameters of plates only and aggregates only are also shown.

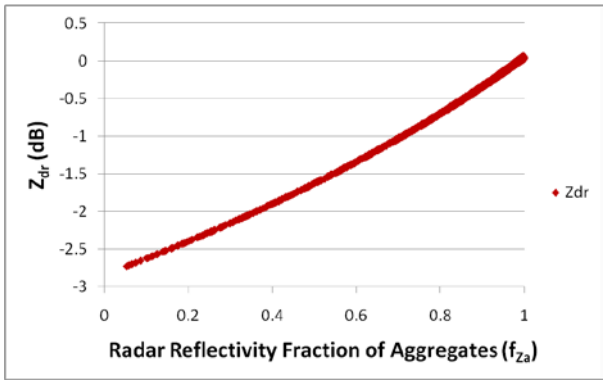

Figure 7. Z_{dr} (dB) of an ice mixture of H-oriented aggregates and V-oriented plates as a function of the radar reflectivity fraction of aggregates (f_{Za}).

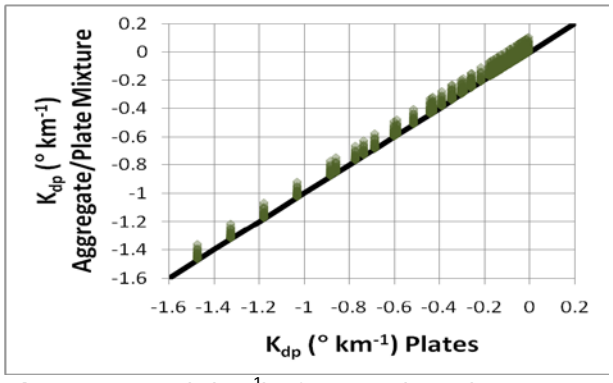

Figure 8. K_{dp} (° km^{-1}) of an H-oriented aggregate and V-oriented plate ice mixture versus K_{dp} of the V-oriented plate only contribution to the mixture.

4.6 K_{dp} and Z_{dr} Dependence on Graupel Properties

In order to understand the dual-polarimetric radar properties of ice mixtures of graupel and crystals, we first characterize the dependence of K_{dp} and Z_{dr} on graupel properties. Graupel particles are modeled as oblate spheroids. Following Bringi et al. (1986), we model the graupel PSD with an exponential distribution in which 1×10^4 m^{-3} cm^{-1} ≤ N0 ≤ 8×10^5 m^{-3} cm^{-1} and 0.08 ≤ D0 ≤ 0.32 cm (D_{max} = 1.0 cm). The shape is specified by setting the minor-to-major axis ratio of the oblate spheroid to 0.75 (Bringi et al. 1986). A range of graupel density is explored by employing both 0.3 g cm^{-3} (low density) and 0.6 g cm^{-3} (moderate density). The orientation of graupel is modeled with a Gaussian distribution of canting angles. Two scenarios are explored, including horizontally (H) oriented (mean canting angle of 0°) and vertically (V) oriented (mean canting angle of 0°). The standard deviation of the canting angle is set to 45° in both cases. It is important to note that the V-orientation is not associated with a strong electric field. Graupel is typically too large and too dense to be aligned by an electric field within a thunderstorm. However, whether oblate graupel falls with major dimension in the horizontal (H-oriented) or in the vertical (V-oriented) is not well known so we model both possibilities here.

For the modeled graupel particles, Z_{dr} is strongly dependent on density but the overall Z_{dr} signature is weak ($|Z_{dr}|$ < 0.2 dB) in all cases (i.e., whether vertically or horizontally oriented and low or moderate density). The K_{dp} signatures are low-to-moderate ($|K_{dp}|$ < 0.8 ° km^{-1}) and strongly dependent on graupel density. For Z_h > 40-45 dBZ, $|K_{dp}|$ is moderate for both H- and V-oriented graupel. For larger horizontal reflectivity (Z_h > 40-45 dBZ), graupel has the potential to mask ice crystal vertical alignment signatures in K_{dp} associated with strong electric fields and lightning potential. The masking potential of graupel in ice mixtures of crystals and graupel particles will be explored further in the next section.

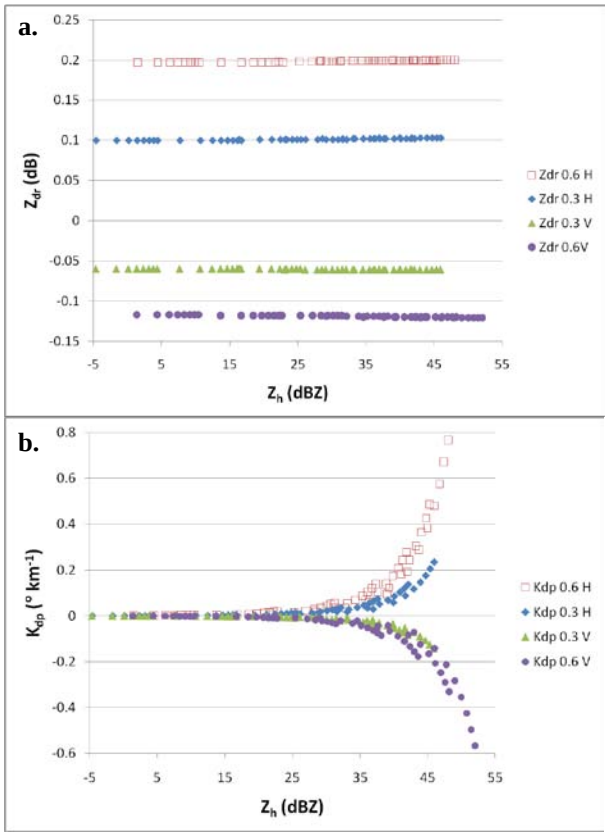

Figure 9. Dual-polarimetric parameter vs. Zh for graupel particles of different types as shown in the key to the right (density, orientation). See text for more model details. a. Z_{dr} (dB) vs. Z_h (dBZ) and b. K_{dp} (° km^{-1}) vs. Z_h (dBZ).

4.7 K_{dp} and Z_{dr} in Mixture of V-oriented Plates and H-oriented Graupel

Next, we explore the dual-polarimetric characteristics of ice crystal and graupel particle mixtures and more specifically the masking potential of graupel in such ice mixtures. Plates are modeled as in earlier sections (Secs. 4.1, 4.3, 4.5). Graupel PSD and shape are modeled as before in Sec. 4.6. To understand the extent of potential graupel masking effects on K_{dp} and Z_{dr}, moderate graupel density (0.6 g cm^{-3}) is assumed.

As horizontal reflectivity of the overall ice mixture (Fig. 10a) and the reflectivity fraction of graupel (f_{Zg}) in the ice mixture (Fig. 11) increase, Z_{dr} of the ice mixture transitions from the intrinsic

value of plates only (about -3 dB) to the intrinsic value of graupel only (about 0.2 dB). Although Z_{dr} in a graupel-plate mixture can vary substantially for a given Z_h ($5 < Z_h < 25$ dBZ, Fig. 10a), there is a minimum Z_{dr} (i.e., a lower envelope to the scatter of points) for each Z_h that depends on f_{Zg} (Fig. 11). For low-to-moderate values of Z_h (10-20 dBZ) in a graupel-plate mixture, Z_{dr} can span the range of values from plate (-3 dB) to graupel (0.2 dB) (Fig. 10a), depending on f_{Zg} (Fig. 11).

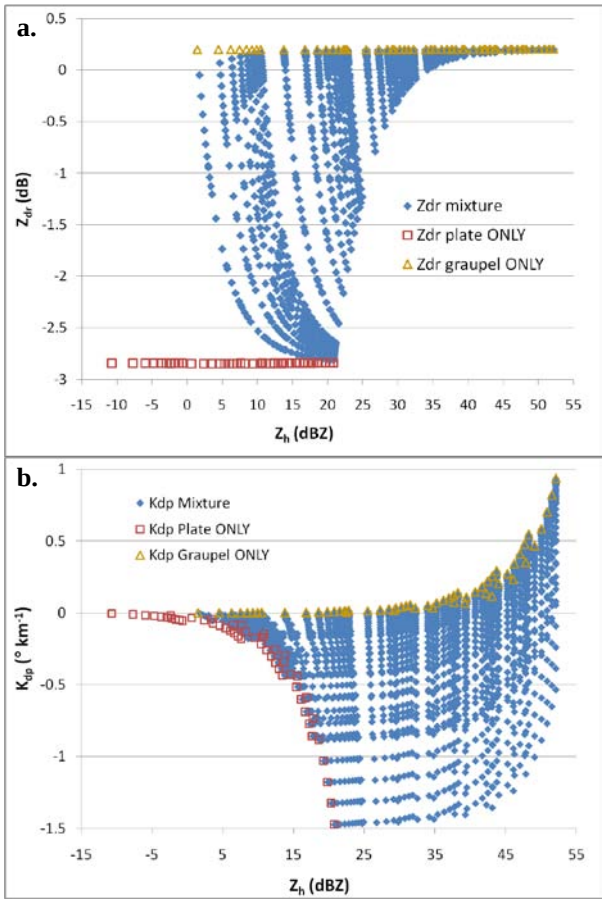

Figure 10. Dual-polarimetric parameter versus Z_h in an ice mixture of H-oriented graupel and V-oriented plates. a. Z_{dr} (dB) vs. Z_h (dBZ) and b. K_{dp} (° km^{-1}) vs. Z_h (dBZ). Plates only and graupel only are also shown.

As with an aggregate-plate mixture (Sec. 4.5), Z_{dr} is a poor indicator of electrical alignment of ice crystals in a graupel-crystal ice mixture because larger, H-oriented graupel particles quickly dominate the smaller, V-oriented plates. This result is expected because Z_{dr} is the reflectivity-weighted measure of particle shape and graupel dominates the reflectivity in most plate-graupel mixtures.

For low-to-moderate values of reflectivity ($5 < Z_h < 35$ dBZ), K_{dp} of a graupel-plate mixture is dominated by the contribution from electrically aligned plates (Figs. 10b, 9b, 4b). A transition occurs from 35 dBZ to 40 dBZ where the intrinsic K_{dp} of H-oriented graupel begins to increase above non-zero values (Figs. 9b, 10b). Note how the lower envelope of Z_{dr} for a given Z_h in a graupel-plate mixture bends upward for $Z_h > 35$ dBZ (Fig. 10b). At $Z_h > 40$-45 dBZ, the $|K_{dp}|$ of H-oriented graupel (Fig. 9b) can be on the order of the $|K_{dp}|$ of V-oriented plates (Fig. 4b). For large values of Z_h (45-52 dBZ), K_{dp} is positive about as often as it is negative in an ice mixture of H-oriented graupel and V-oriented plates. Clearly, in a graupel-plate mixture, horizontally oriented graupel can mask the electrical alignment signature that would otherwise be present in the K_{dp} of V-oriented plates alone (Fig. 12). This masking effect occurs primarily at moderate-to-large values of horizontal reflectivity (Fig. 10b).

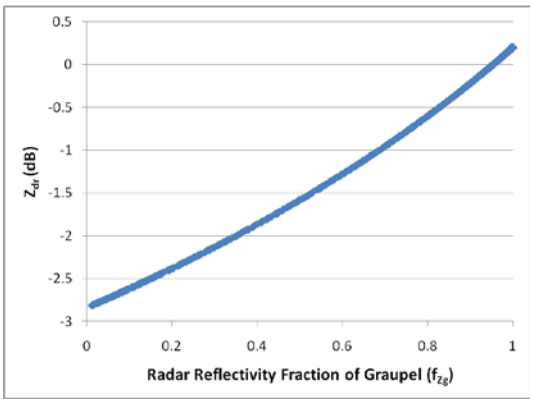

Figure 11. Z_{dr} (dB) of an ice mixture of H-oriented graupel and V-oriented plates as a function of the radar reflectivity fraction of graupel (f_{Zg}).

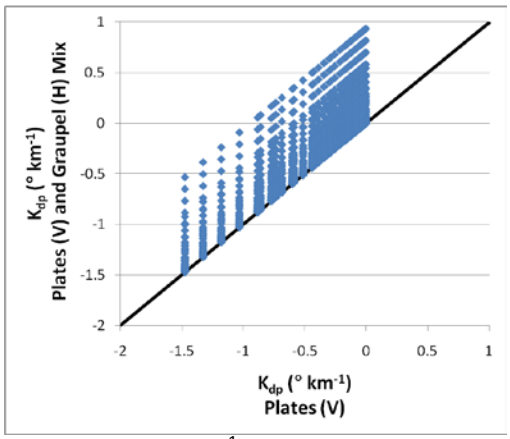

Figure 12. K_{dp} (° km^{-1}) of an H-oriented graupel and V-oriented plate ice mixture versus K_{dp} of the V-oriented plate only contribution to the mixture.

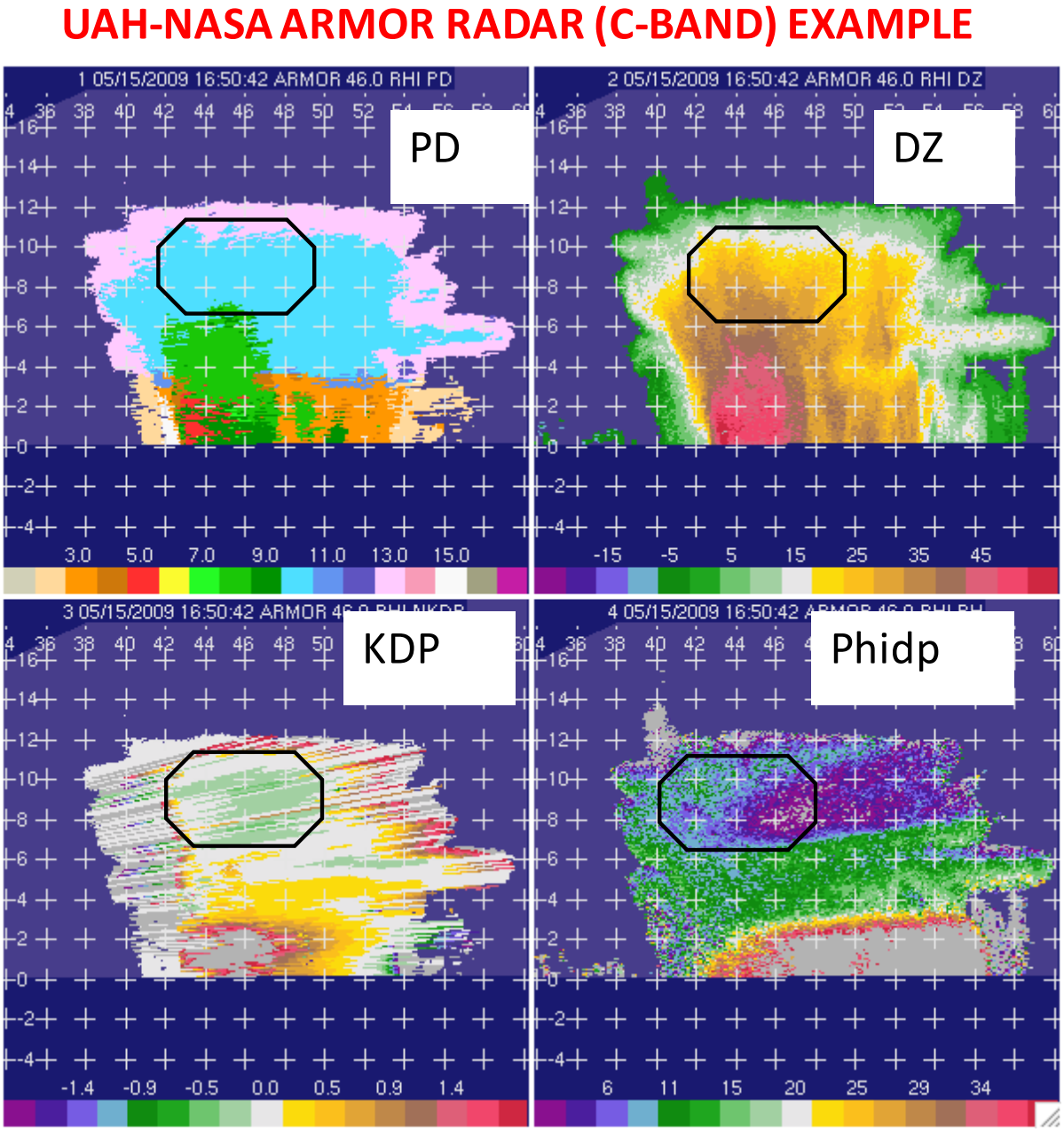

Figure 13. RHIs (height vs. range in km) of ARMOR dual-polarimetric radar signatures of oriented ice (within region highlighted by a circle) on May 15th 2009 during the mature phase of a thunderstorm (1651 UTC) over Northern Alabama. Clockwise from upper left: hydrometeor identification (PD), horizontal reflectivity (DZ), specific differential phase (KDP), and differential propagation phase (Phidp). See text for discussion and details.

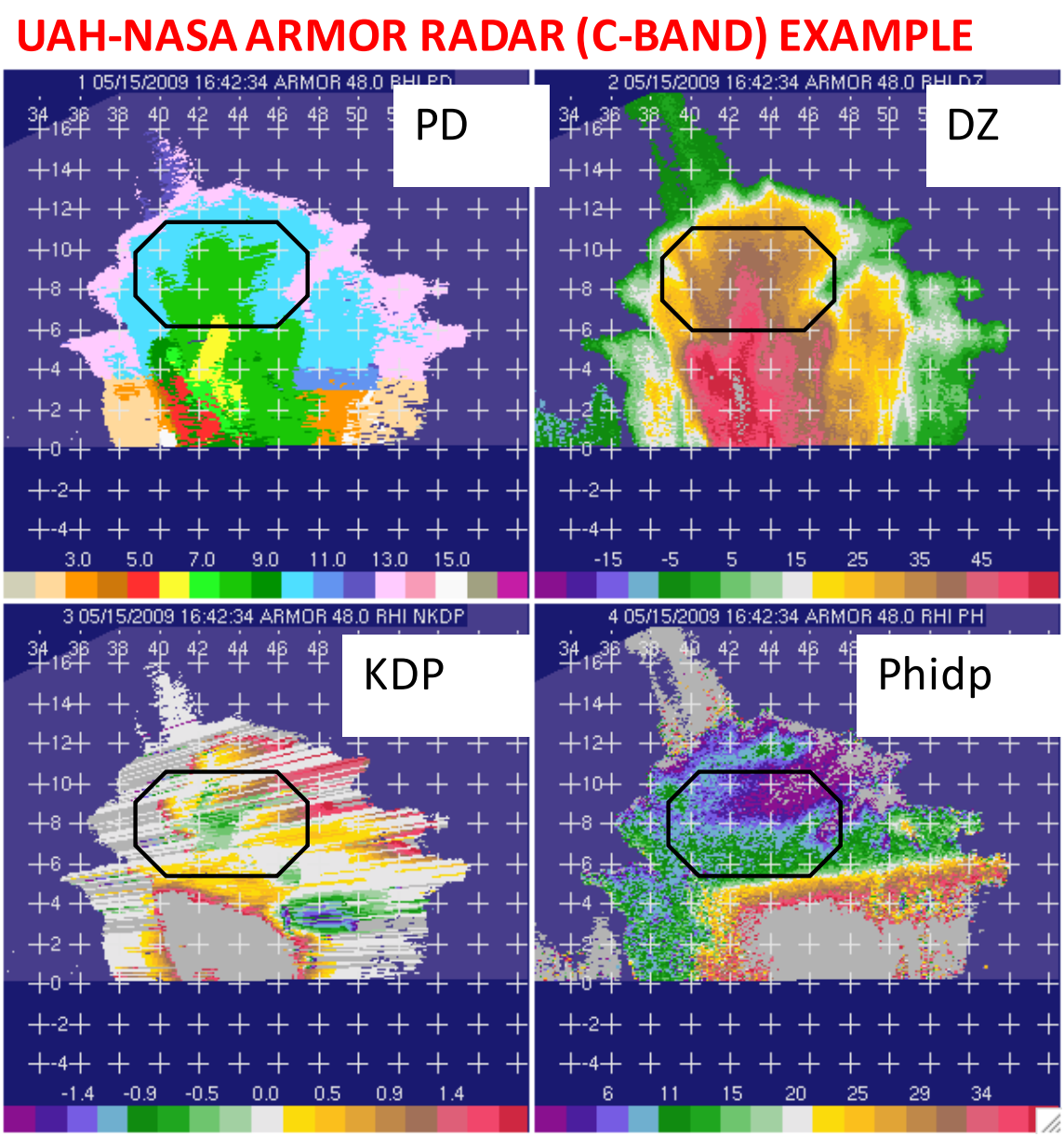

Figure 14. Same as Figure 13 except eight minutes earlier in the cell lifecycle (1643 UTC) when the thunderstorm was more intense. See text for discussion and details.

4.8 ARMOR Examples of PHIDP/K_{dp} Electrical Alignment Signatures

ARMOR RHI examples of PHIDP and K_{dp} that are likely electrical alignment signatures are shown in Figs. 13 and 14. In Fig. 13, the K_{dp}/PHIDP alignment signatures (circled region, bottom row) are above and slightly down wind of the convective core. The differential phase alignment signatures are in low-to-moderate reflectivity (DZ: 20-30 dBZ, top right, Fig. 13) within "dry snow" as identified by a fuzzy-logic based dual-polarimetric particle identification (PD=light blue, top left, Fig. 13). Since dual-polarimetric particle identification algorithms have known deficiencies in detecting mixtures of ice (e.g., snow and crystals) and tend to provide reflectivity weighted results (e.g., would identify a snow/crystal mixture as snow only), ice crystals are likely in the circled region too with the negative K_{dp} and PHIDP. In fact, negative differential phase may be the proof that ice crystals are there. Although we cannot rule out vertically oriented dry snow causing the negative PHIDP, our simulation results are inconsistent with that conclusion. In summary, Fig. 13 provides an example of negative K_{dp} (negative PHIDP) that is consistent with electrical alignment of ice-crystals and/or snow into the vertical.

Fig. 14 depicts the same cell just 8 minutes earlier when it was more intense. For this earlier time, the negative K_{dp}/PHIDP signatures (circle area, bottom row, Fig. 14) are in and above the convective core in moderate-to-high reflectivity (DZ: > 40-45 dBZ, top right, Fig. 14). The negative differential phase signatures are in "graupel" as identified by dual-polarimetric particle identification (PD=green, top left, Fig. 14). As discussed before, the particle identification algorithms tend to be dominated by the largest particle so ice crystals are likely also present with graupel. However, based on model simulations, it is unclear as to whether these negative K_{dp}/PHIDP signatures are associated with vertically oriented ice crystals in a strong electric field, graupel falling with major axis in the vertical (V-oriented graupel) or both. Regardless of the answer, it is likely that a strong electric field is present and the negative phase signature is at least partially associated with it.

5. SUMMARY

- K_{dp} related linearly to N0 (concentration) and non-linearly to D0 (size) of an exponential size distribution of ice particles.
- K_{dp} weakly sensitive to ice crystal type (plates, columns same; dendrites 15-30% less).
- K_{dp} signatures of ice aggregates (low density) are small compared to ice crystals.
- In an aggregate-ice crystal mixture, K_{dp} (propagation-based) is a good indicator of E-field alignment because smaller, V-oriented ice particles dominate in a mixture of V-oriented crystals and H-oriented aggregates.
- Z_{dr} (backscatter-based) is a poor indicator of electrical alignment in a mixture of V-oriented ice crystals and H-oriented ice aggregates because it is a reflectivity-weighted measure of shape and orientation. So, the larger aggregates, whose orientation is likely unrelated to E-field, tend to dominate Z_{dr}.
- $|K_{dp}|$ is moderate-to-large for H- and V-oriented graupel at Z_h > 40-45 dBZ. Since graupel orientation likely NOT connected to E-field, large graupel could "mask" or "enhance", respectively, ice crystal orientation signatures due to E-field in moderate to high dBZ.
- Being a propagation-based measure does not make K_{dp} immune from "masking" effects in mixtures. It depends on ice properties.
- Larger N0 for V-crystal aloft and H-graupel masking below likely explain why K_{dp}/PHIDP signature is often limited to top of convective cell and anvil, even though ice crystals, strong E-field and lightning do occur in strong dBZ below (earlier example).
- Electric field threshold for vertical alignment of ice crystals is related to particle size (D0), shape and density. Hence, electric field and *lightning potential* are physically connected to the PHIDP/K_{dp} alignment signature.
- Quantitative use of will likely be elusive due to ambiguities associated with ice particle characteristics/microphysics, electric field strength, and radar observational errors.
- Likely limited to qualitative use: e.g., as part of a radar or multi-sensor fuzzy logic-based probabilistic lightning potential product (Deierling et al. 2009)

6. REFERENCES

Auer, A. H., and D. L. Veal, 1970: The dimension of ice crystals in natural clouds. *J. Atmos. Sci.*, **27**, 919-926.

Brown, P. R. A., and P. N. Francis, 1995: Improved measurements of the ice water content in cirrus using a total-water probe. J. Atmos. Oceanic Technol., 12, 410-414.

Carey, L. D., and S. A. Rutledge, 1996: A multiparameter radar case study of the microphysical and kinematic evolution of a lightning producing storm. *Meteor. Atmos. Phys.*, **59**, 33–64.

Caylor, I. J., and V. Chandrasekar, 1996: Time-varying ice crystal orientation in thunderstorms observed with multiparameter radar. IEEE Trans. Geosci. Remote Sens., 4, 847-858.

Deierling, W., Latham, J., W. A. Petersen, S. M. Ellis, and H. J. Christian Jr., 2005: On the relationship of thunderstorm ice hydrometeor characteristics and total lightning measurements. *Atmos. Res.*, **76**, 114-126.

Galloway, J., A. Pazmany, J. Mead, R. E. McIntosh, D. Leon, J. French, R. Kelly, and G. Vali, 1997: Detection of ice hydrometeor alignment using an airborne W-band polarimetric radar. *J. Atmos. Oceanic Technol.*, **14**, 3-12.

Garrett, T. J. and co-authors, 2005: Evolution of a Florida cirrus anvil. *J. Atmos. Sci.,* **62**, 2352-2372.

Harms, D. E., A. A. Guiffrida, B. F. Boyd, L. H. Gross, G. D. Strohm, R. M. Lucci, J. W. Weems, E. D. Priselac, K. Lammers, H. C. Herring and F. J. Merceret, 1999: The Many Lives Of A Meteorologist In Support Of Space Launch, *8th Conference On Aviation, Range, and Aerospace Meteorology,* 10-15 Jan 99, 5-9.

Hendry, A., and G. C. McCormick, 1976: Radar observations of the alignment of precipitation particles by electrostatic fields in thunderstorms, *J. Geophys. Res.*, **81**, 5353-5357.

Hendry, A., and Y. M. M. Antar, 1982: Radar observations of polarization characteristics and lightning-induced realignment of atmospheric ice crystals, *Radio Sci.*, **17**, 1243-1250.

Heymsfield, A. J., 1972: Ice crystal terminal velocities. *J. Atmos. Sci.,* **29**, 1348-1357.

Heymsfield, A. J., 1986: Ice particle evolution in the anvil of a severe thunderstorm during CCOPE. *J. Atmos. Sci.,* **43**, 2463-2478.

Huffines, G. R., and R. E. Orville, 1999: Lightning Ground Flash Density and Thunderstorm Duration in the Continental United States: 1989-96. *J. Appl. Meteor.*, **38,** 1013-1019.

Krehbiel, P. R., W. Rison, S. McCrary, T. Blackman, and M. Brook, 1991: Dual-polarization radar observations of lightning echoes and precipitation alignment at 3 cm wavelength. *25th Int. Conf. Radar Meteor.*, Amer. Meteor. Soc., Boston, MA, 901-904.

Krehbiel, P. R., T. Chen, S. McCrary, W. Rison, G. Gray, T. Blackman, and M. Brook, 1992: Dual-polarization radar signatures of the potential for lightning in electrified storms. *9th Int. Conf. Amos. Elect.*, St. Petersburg, Russia, 166-169.

Krehbiel, P. R., T. Chen, S. McCrary, W. Rison, G. Gray, and M. Brook, 1993: Dual-polarization radar indications of the potential for lightning in storms near Kennedy Space Center, Florida. *26th Conf. Radar Meteor.*, Amer. Meteor. Soc., Boston, MA, 309-311.

Krehbiel, P. R., T. Chen, S. McCrary, W. Rison, G. Gray, and M. Brook, 1996: The use of dual channel circular-polarization radar observations for remotely sensing storm electrification. *Meteor. Atmos. Phys*., **59**, 65-82.

Marshall, T. C., M. Stolzenburg, P. R. Krehbiel, N. R. Lund, and Chris R. Maggio, 2009: *J. Geophys. Res.*, **114**, D02209, doi:10.1029/2008JD010637.

Matrosov, S. Y., 1991: Theoretical study of radar polarization parameters obtained from cirrus clouds. *J. Atmos. Sci.*, **48**, 1062-1070.

Matrosov, S. Y., R. F. Reinking, R. A. Kropfli, and B. W. Bartram, 1996: Estimation of ice hydrometeor types and shapes from radar polarization measurements. *J. Atmos. Oceanic Technol.*, **13**, 85-96.

McCormick, G. C., and A. Hendry, 1979: Radar measurements of precipitation-related depolarization of thunderstorms. *IEEE Trans. Geosci. Electron.*, **GE-17**, 142-150.

Metcalf, J., 1992: Radar observations of the effects of changing fields on the orientations of hydrometeors. Phillips Lab, Air Force Syst. Command, Hanscom AFB, MA PL-TR-92-2122, ERP 1100, p. 30.

Metcalf, J., 1995: Radar observations of changing orientations of hydrometeors in thunderstorms. *J. Appl. Meteor.*, **34**, 757-772.

Petersen, W. A., K. Knupp, J. Walters, W. Deierling, M. Gauthier, B. Dolan, J. P. Dice, D. Satterfield, C. Davis, R. Blakeslee, S. Goodman, S. Podgorny, J. Hall, M. Budge, and A. Wooten: The UAH-NSSTC/WHNT ARMOR C-Band dual polarimetric radar: A unique collaboration in research, education, and technology transfer. Preprints, *32nd Conference on Radar Meteorology*, Albuquerque, New Mexico, 24-29 October 2005.

Pruppacher, H. R., and J. D. Klett, 1997: Microphysics of clouds and precipitation. 2nd Edition, Kluwer Academic Publishers, 954 pp.

Roeder, W. P., and C. S. Pinder, 1998: Lightning Forecasting Empirical Techniques For Central Florida In Support Of America's Space Program, *16th Conference on Weather Analysis and Forecasting*, 11-16 Jan 98, 475-477.

Roeder, W. P., T. M. McNamara, B. F. Boyd, and F. J. Merceret, 2009: The New Weather Radar for America's Space Program in Florida: An Overview, *34th Conference on Radar Meteorology*, 5-9 Oct 09, Paper 10B.6.

Ryzhkov, A. V., D. S. Zrnic, and B. A. Gordon, 1998: Polarimetric method for ice water content determination. *J. Appl. Meteor.*, **37**, 125-134.

Scott, R. D., P. R. Krehbiel, and W. Rison, 2001: The use of simultaneous horizontal and vertical transmissions for dual-polarization radar meteorological observations. *J. Atmos. Oceanic Technol.*, **18**, 629-648.

Vivekanandan, J., W. M. Adams, and V. N. Bringi, 1991: Rigorous approach to polarimetric radar modeling of hydrometeor orientation distributions. *J. Appl. Meteor.*, 30, 1053-1063.

Vivekanandan, J., R. Raghavan, and V. N. Bringi, 1993: Polarimetric radar modeling of mixtures of precipitation particles. *IEEE Trans. Geosci. Remote Sens.*, **31**, 1017-1030.

Vivekanandan, J. V. N. Bringi, M. Hagen, and P. Meischner, 1994: Polarimetric radar studies of atmospheric ice particles. *IEEE Trans. Geosci. Remote Sens.*, **32**, 1-10.

Weinheimer, A. J., and A. A. Few, 1987: The electrical field alignment of ice particles in thunderstorms. *J. Geophys. Res.*, **92**, 14,833-14,844.